ELSEVIER

Geotextiles and Geomembranes 19 (2001) 23–44

Geotextiles and Geomembranes

www/elsevier.com/locate/geotexmem

Centrifugal and numerical modelling of reinforced embankments on soft clay installed with wick drains

J.S. Sharma[a,*], M.D. Bolton[b]

[a]*Swiss Federal Institute of Technology, Zurich, Switzerland*

[b]*Cambridge University Engineering Department, Trumpington Street, Cambridge CB2 1PZ, UK*

Received 14 February 2000; received in revised form 24 June 2000; accepted 8 July 2000

Abstract

Centrifuge models and finite element analyses of reinforced embankments on soft clay (with or without wick drains) are presented. The results obtained from the centrifuge tests were compared with those from the finite element analyses and were found to be in good agreement. For the case of reinforced embankments on soft clay installed with wick drains, it was found that the magnitude of maximum tension in the reinforcement was slightly higher than that for the case of no wick drains. Also, the distribution of tension in the reinforcement was much more localised under the shoulder of the embankment for the wick drain case as compared to the case of no wick drains. Base reinforcement of embankment is effective in situations, where the demanded shear strength of the clay foundation marginally exceeds the available shear strength. The presence of wick drains in soft clay increases the strength of the clay foundation significantly during the period of embankment construction. This gain in shear strength ensures better mobilization of tension in the reinforcement and contributes significantly towards the stability of the embankment.

Keywords: Embankment; Soft clay; Geotextile reinforcement; Wick drains; Centrifuge modelling; Finite element modelling

* Correspondence address: Institute for Geotechnical Engineering, ETH Hönggerberg/HIL, CH-8093 Zurich, Switzerland.

E-mail addresses: jitendra@igt.baug.ethz.ch (J.S. Sharma), mdb@eng.cam.ac.uk (M.D. Bolton).

0266-1144/01/$ - see front matter
PII: S0266-1144(00)00009-1

1. Introduction

Embankments on soft clays are often required when building roads, railways or flood control structures. The lowest margin of safety of an embankment constructed over soft soil is at the end of its construction when the loading is at its maximum and the strength of the soil is significantly reduced due to the generation of high excess pore pressures. The long-term stability of such embankments is usually satisfactory because of the gain in strength of the subsoil due to consolidation. Therefore, short-term instability controls their design.

Several techniques are available for enhancing the stability of embankments. The most commonly used technique is the staged construction of the embankment which sometimes is used in combination with the installation of wick drains in soft clay to increase the rate of consolidation under the embankment loading. However, in recent years, the technique of reinforcing the embankment at the base using a geosynthetic fabric to improve its short-term stability has become popular. The idea is to resist the lateral thrust in the embankment and the lateral deformation of the subsoil by the tension induced in the reinforcement. This technique is widely used now-a-days and data are available from several instrumented field trials (Bassett and Yeo, 1988; Rowe et al., 1995). Sophisticated numerical analyses (Rowe and Mylleville, 1989; Hird and Pyrah, 1991; Sharma and Bolton, 1996) have also helped to clarify the behaviour of reinforced embankments on soft clays.

In situations where the clay foundation has insufficient bearing capacity, it may be advantageous to use base reinforcement of the embankment in combination with the installation of wick drains in the clay foundation. The behaviour of such embankments is complex and their design is made more difficult by a general lack of data either from field trials or from numerical analyses. One reason for the dearth of numerical modelling of such embankments may be the fact that most embankment analyses are carried out on the assumption of plane strain conditions whereas the consolidation of soil around each wick drain is closer to that of axial symmetry. Therefore, in order to incorporate the effects of wick drains, a procedure for matching their effect under axisymmetric and plane strain conditions is necessary. One such procedure has been proposed by Hird et al. (1992) which permits the matching of the average degree of consolidation at all times and at all depths in the soil. However, the validity of this procedure has only been checked using the results from field trials (Hird et al., 1992, 1995) which are notoriously difficult to interpret. They tend to suffer from poor quality control at the site, a hazardous environment causing malfunctioning of the instrumentation and variable site conditions that are difficult to incorporate in numerical analyses. It is even difficult to obtain a fair comparison between the results of two similar field trials carried out at adjacent sites. On the other hand, centrifuge model testing, because of its ability to reproduce same stress levels in a small-scale model as in a full-scale prototype, is a powerful tool in exploring such complex soil–structure interaction problems. Idealised conditions may be created in centrifuge models to facilitate the validation of analytical or numerical solutions. Furthermore, centrifuge modelling offers the advantage of ease of management, repeatability, greater control over the entire event, well-defined soil

properties, shorter consolidation time-scale and the option to continue the test up to failure.

In this paper, the behaviour of reinforced embankments on soft clay (with and without wick drains) has been explored using centrifugal as well as finite element modelling. The objectives of this paper are two-fold: (a) to examine the validity of the matching procedure suggested by Hird et al. (1992), and (b) to explore the role of wick drains in improving the stability of the embankment when used in combination with the base reinforcement.

2. Centrifuge tests — equipment and procedure

In the present study, three 1 : 40 scale centrifuge model tests were performed using the Cambridge University 10 m balanced beam centrifuge. Fig. 1 shows the details of a typical centrifuge model. Table 1 gives a summary of each of the three tests. Detailed description of centrifuge test equipment and procedure can be found in Sharma (1994) and Bolton and Sharma (1994). Due to the inherent symmetry of the embankment about its centreline, only one half of it was modelled. Such an arrangement helped in

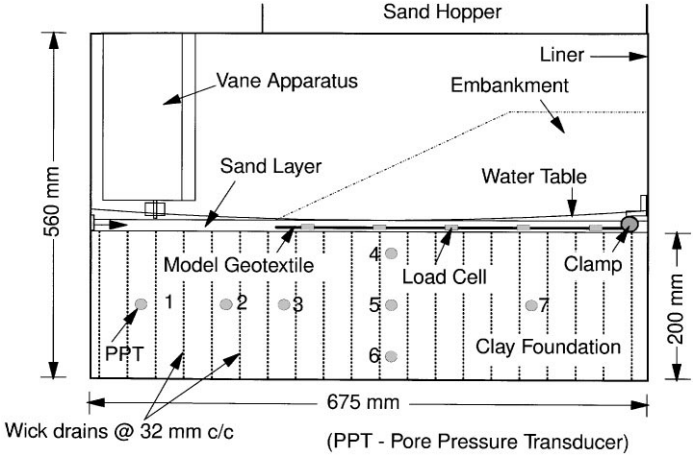

Fig. 1. Arrangement of model for a typical centrifuge test.

Table 1
Details of centrifuge tests

Test code	Depth of clay (mm)	Reinforcement	Wick drains
JSS7	200	Geotextile	Not present
JSS8	200	Unreinforced	Not present
JSS14	200	Geotextile	Present

constructing a model of reasonable size within a relatively small strongbox. A special clamp was built to anchor the model reinforcement to the right side of the liner. This clamp, while preventing the horizontal movement of the reinforcement, allowed for its downward vertical movement following the settlement of the clay foundation.

A smooth nylon sheet was glued to the inside vertical surfaces of the strongbox liner and was coated with a thin film of silicone grease to reduce the friction between the liner and the soil. The Speswhite kaolin clay slurry was consolidated to a maximum vertical pressure of 100 kPa in a consolidometer. Seven miniature pore pressure transducers (PPTs) were installed at various locations in the clay foundation as shown in Fig. 1. While installing PPTs for the clay foundation installed with wick drains, care was taken to ensure that none of the PPTs had its face close to a wick drain. Two days before the day of the centrifuge test, it was unloaded and removed from the consolidometer and was trimmed to the dimensions of the model. An array of black plastic markers was installed on the front face of the clay block. This was used for measuring clay displacements from photographs taken in-flight through the front perspex window.

As indicated in Table 1, wick drains were installed in the clay foundation for test JSS14. Only a brief description of the wick drain will be given here. The details of wick drain installation can be found in Sharma (1994). A twisted multifilament polyester string having 1.5 mm nominal diameter modelled the wick drains. The transmissivity or permeability of this string was measured using a customised band drain permeameter (Broms et al., 1994) and was found to be approximately 2.0×10^{-4} m/s at 70 kPa of confining pressure. This value compares favourably with transmissivity of some of the commercially available composite band drains. A square layout with 32 mm c/c spacing was chosen. At a centrifugal acceleration of 40 g, the model wick drain was equivalent to a prototype 150 mm wide, 16 mm thick band drain spaced at 1.3 m c/c.

A multifilament woven polyester model geotextile manufactured specially for the present study was used as the reinforcement. The process of scaling-down the prototype reinforcement to obtain the model reinforcement has been discussed in detail by Springman et al. (1992). At 40 g, the model geotextile represented a prototype geotextile having a tensile strength of 380 kN/m at 10% axial strain. For the measurement of tensile force mobilised during and after embankment construction, five load cells were constructed on the model geotextile. The details of the load cells and the procedure and results of their calibration can be found in Bolton and Sharma (1994). Before loading the model on the centrifuge, the model geotextile with calibrated load cells was attached to the clamp and was placed directly on top of the model clay foundation. A 10 mm thick layer of Leighton–Buzzard 25/52 sand was then placed uniformly over the reinforcement.

2.1. Vane shear strength profile of the clay foundation

After bringing the clay foundation to a state of hydrostatic equilibrium at 40 g, in-flight vane shear tests were conducted at various depths using the miniature vane shear apparatus. The site chosen for these tests was sufficiently away from the site of

embankment. The width of the miniature vane was 18 mm and its height was 14 mm. Almeida and Parry (1983) give the reasons for choosing these dimensions for the miniature vane. Fig. 2(a) shows a typical shear stress vs. vane rotation plot for test JSS7. It should be noted that the peak vane shear strength is obtained by subtracting the contribution of the vane shaft from the maximum value of the shear strength as shown in Fig. 2(a). The variation of peak vane shear strength (s_{uv}) with depth for the three tests is shown in Fig. 2(b). The following correlation between the peak vane shear strength measured by the miniature vane shear apparatus, the vertical effective stress at the test site and the overconsolidation ratio (OCR) has been established from several centrifuge model tests using kaolin (Almeida and Parry, 1983; Phillips, 1988; Springman, 1989):

$$\frac{s_{uv}}{\sigma'_v} = a(OCR)^b, \tag{1}$$

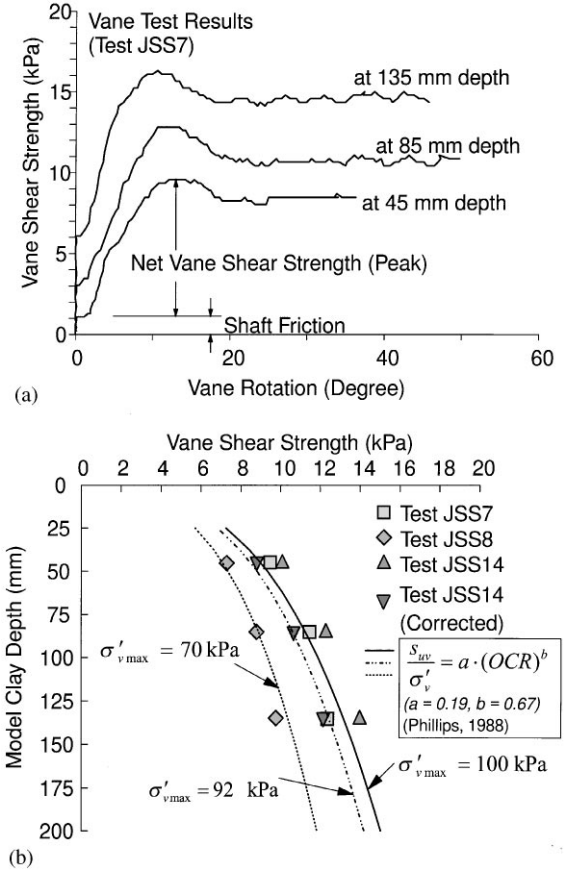

Fig. 2. (a) Vane shear test results for test JSS7. (b) Vane shear strength profiles for the clay foundation.

where $a = 0.19$ and $b = 0.67$ (Phillips, 1988). The variation of s_{uv} with depth obtained from Eq. (1) is also shown in Fig. 2(b). It can be seen that the results for test JSS7 are consistent with those calculated from Eq. (1). However, the results for test JSS8 are lower and the results for test JSS14 (with wick drains) are higher than those calculated from Eq. (1).

Sharma (1994) has described the reason for lower vane shear strength of clay foundation for test JSS8 in detail. It was due to loss of initial pore suction in clay foundation that is usually present before it is subjected to centrifugal acceleration. This loss of pore suction was due to significant amount of water that was accidentally sucked in from the standpipe connected to the bottom drain and was accompanied by swelling of the clay foundation. As a result, the clay foundation behaved as though it was precompressed to a vertical stress that was considerably less than the design value of 100 kPa. From Fig. 2(b), it can be seen that the vane shear strength profile for test JSS8 matches the one calculated from Eq. (1) only when the value of maximum preconsolidation pressure is reduced to 70 kPa.

The higher vane shear strengths obtained for test JSS14 can be explained on the basis of the permeability of the clay foundation and the rate of vane rotation. For all the vane shear test results shown in Fig. 2(b), the rate of vane rotation was 1.1°/s and the peak vane shear strength was reached at around 15 to 20° vane rotation. Therefore, the time taken to reach the peak vane shear strength was approximately 14–18 s. Blight (1968) has proposed the following equation that relates the degree of consolidation with time taken to mobilise full vane shear strength:

$$U = 1 - \frac{1}{T}\left[\frac{1}{8} + \frac{4}{\pi^3}\sum_{n=1}^{\infty}\frac{(-1)^n}{n^3}\sin\left(\frac{n\pi}{2}\right)e^{-\pi^2 n^2 T}\right], \tag{2}$$

where T is the time factor defined as

$$T = \frac{c_v t_f}{D^2}, \tag{3}$$

and D is the width of the vane blade, c_v is the coefficient of consolidation of clay and t_f is the time taken to reach peak vane shear strength. Eqs. (2) and (3) can not be applied directly to clays installed with wick drains because of rather complex drainage boundary conditions. However, for such cases, the assessment of the extent of drainage during the vane shear test can be made using an equivalent value of c_v estimated from the variation of excess pore pressure with time underneath the embankment during and after its construction as shown in Fig. 3(a). It should be noted that the equivalent c_v value so obtained has no physical significance. For test JSS7, c_v was found to be 0.43 m^2/day and for test JSS14, it was found to be 1.96 m^2/day. It should be emphasised that this procedure gives the equivalent c_v for test JSS14 that is significantly higher than that for test JSS7 due to the presence of wick drains. Using these values of c_v along with $t_f = 18$ s in Eqs. (3) and (2), we obtain $U = 3\%$ for test JSS7 and $U = 26\%$ for test JSS14. It is fairly obvious that for test JSS14, undrained conditions could not be sustained during the vane shear testing and as a result, higher vane shear strengths were recorded. However, the undrained vane

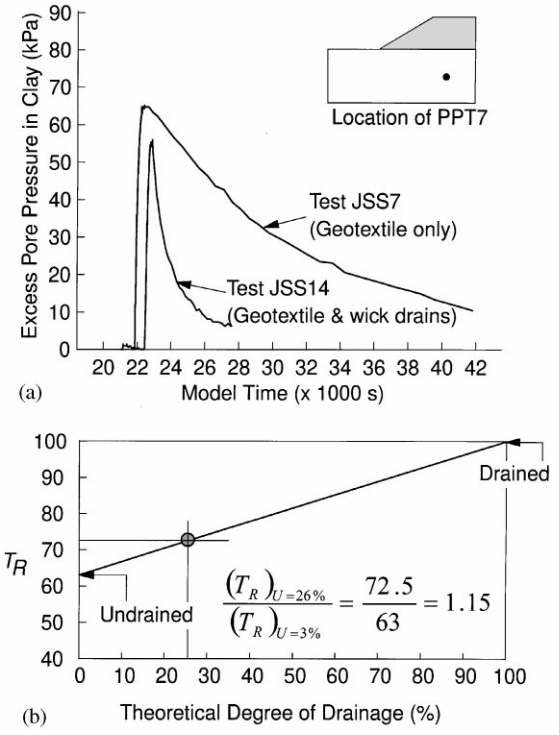

Fig. 3. (a) Excess pore pressures in the clay foundation during and after embankment construction. (b) Estimation of correction factor for the degree of drainage during a vane shear test (test JSS14).

shear strength profile for test JSS14 can be obtained with the help of Fig. 3(b) (reproduced from Blight, 1968) which shows variation of theoretical degree of drainage as given by Eq. (2) plotted against the shear torque as a percentage of torque at the slowest test rate (T_R). From Fig. 3(b), it can be inferred that the shear torque required for full mobilisation of peak vane shear strength for test JSS14 was 1.15 times higher than that required under undrained conditions. Therefore, the undrained vane shear strength profile for test JSS14 was obtained by dividing the measured vane shear strength values by 1.15 and is shown in Fig. 2(b). It can be seen that the undrained vane shear strengths for test JSS14 were marginally smaller than those obtained for test JSS7.

3. Centrifuge tests — summary of results

As expected, the clay foundation installed with wick drains (test JSS14) reached the state of hydrostatic pore pressure equilibrium in a significantly shorter time duration (approx. 2 h) than that taken by the clay foundation without wick drains (approx. 6 h).

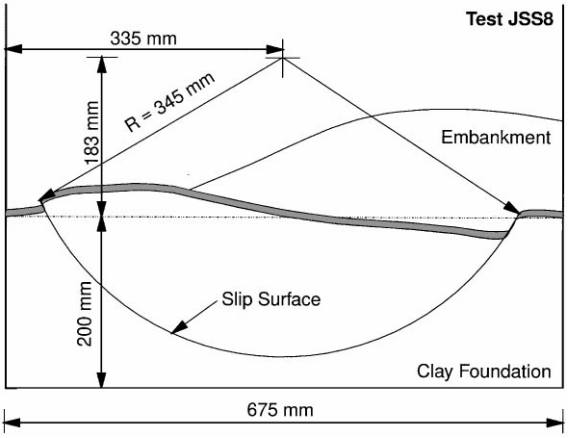

Fig. 4. Failure of unreinforced embankment on soft clay (test JSS8).

Rapid construction of the embankment caused significant deformation of the clay foundation. Excess pore pressures in the clay and the tension in the reinforcement both increased as the embankment construction progressed. The clay foundation for the unreinforced embankment (test JSS8) experienced a classic slip circle failure when about 85% of the total weight of sand in the hopper was placed on the clay layer as shown in Fig. 4 obtained from in-flight photographic measurements. Lateral displacements of upto 3.6 mm were recorded in the clay foundation for test JSS7 whereas only upto 2.6 mm lateral displacements were observed for test JSS14 (Fig. 5). The magnitude of excess pore pressures was less for test JSS14 compared with test JSS7. Maximum tension recorded at the end of embankment construction was 1.5 kN/m for test JSS7 and 2.0 kN/m for test JSS14. It should be noted that these tensions are presented at model scale; they should be multiplied by an appropriate scale factor of 40 in order to obtain the results for a prototype reinforcement of 40 times the stiffness and strength.

4. Finite element modelling

The analyses presented here were conducted using the finite element program CRISP (Britto and Gunn, 1990). Fig. 6 shows the details of the finite element mesh used in these analyses. It is a two-dimensional plane strain mesh with boundary conditions similar to those of a typical centrifuge model with all dimensions 40 times those of the centrifuge model. The clay foundation was modelled using 415 eight-noded linear strain quadrilateral and 39 six-noded linear strain triangular elements with both displacement and pore pressure as unknowns (coupled consolidation type). The embankment was modelled using 343 six-noded linear strain triangular elements with displacement unknown (drained type). The simulation of in-flight

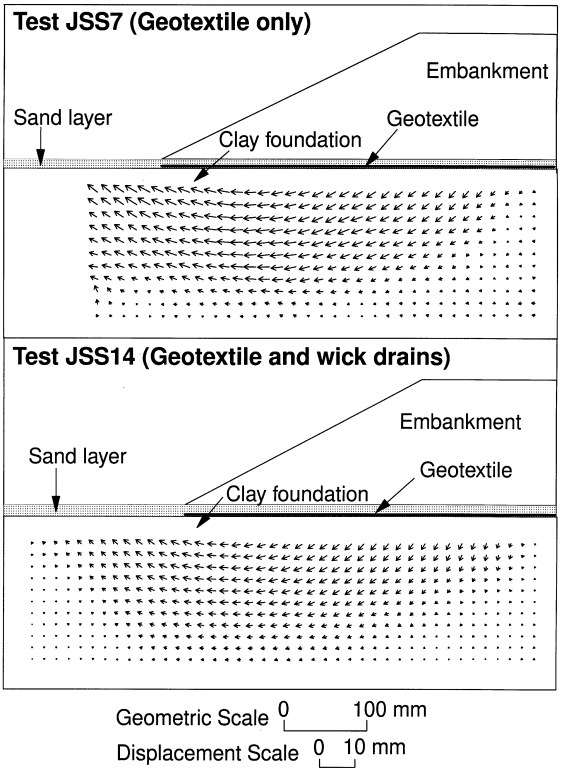

Fig. 5. Deformation of the clay foundation at the end of embankment construction (tests JSS7 and JSS14).

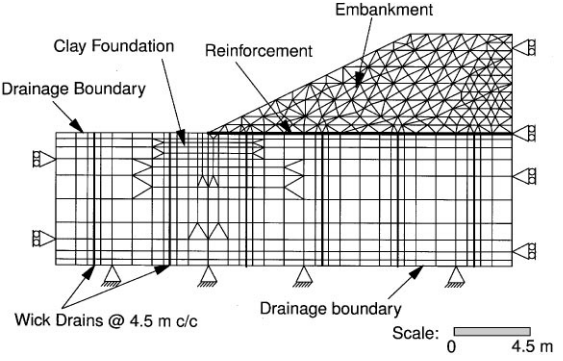

Fig. 6. Details of the finite element mesh.

embankment construction was achieved by adding the elements representing the embankment to the mesh in six layers. There was no waiting period between each successive embankment layer. The profile of embankment after placement of each layer resembled closely with the profile obtained in the centrifuge test. The

geotextile reinforcement was modelled using 25 linear elastic bar elements. The soil–reinforcement interfaces were modelled using 50 six-noded quadrilateral interface elements of the type developed by Goodman et al. (1968) with a Mohr–Coulomb failure criterion. Wick drains were modelled as drainage boundaries with zero-excess pore pressure condition implying zero well resistance. Two unit cell axisymmetric finite element analyses — one with zero well resistance and one with well resistance — were conducted to explore the effect of this assumption. It was found that the use of zero well resistance into finite element analyses did not result in any appreciable loss in accuracy of the results. This is because of the fact that the hydraulic conductivity of the model wick drain used in centrifuge tests was quite high as compared to the permeability of the clay foundation.

4.1. Modelling the behaviour of clay foundation

It is generally well-understood that a one-dimensionally consolidated clay exhibits stress-induced anisotropy. The undrained shear strength (s_u) value for such a clay reduces by as much as 50% as the direction of principal stress changes from nearly vertical in the active zone to nearly horizontal in the passive zone (Ohta et al., 1985). Such behaviour can be modelled accurately only when an anisotropic constitutive model is used to represent the clay foundation. However, the use of anisotropic constitutive models is not very common and typically, an isotropic soil model with an average value of s_u (usually obtained from direct simple shear tests) is used when analysing reinforced embankments on soft clay. It has been experimentally observed by several research workers (e.g. Ladd and Foott, 1974; Prevost, 1979) that the s_u value obtained from direct simple shear (DSS) test is the average of s_u values obtained from triaxial compression (active) and extension (passive) tests and it is approximately equal to 75% of the s_u values obtained from a triaxial compression test. Ohta et al. (1992) have also pointed out that for 1D consolidated clays the s_u values obtained from vane shear tests are approximately 15–20% lower than those obtained from DSS tests.

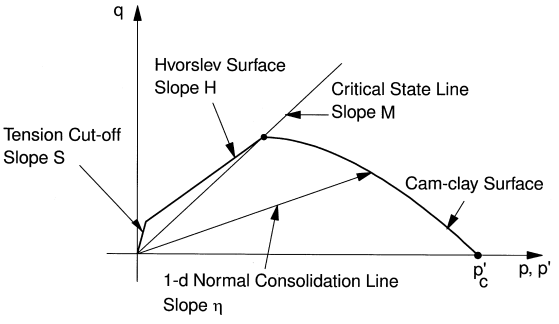

Fig. 7. The Schofield model (after Britto and Gunn, 1990).

In the analyses presented here, the clay foundation is modelled using the Schofield model (Schofield, 1980) — a Cam-clay model with a Hvorslev surface and a tension cut-off on the dry side of the critical state line as shown in Fig. 7. The choice of the Schofield model was influenced by the fact that the clay foundation was heavily overconsolidated at the top with OCR ranging from 33 at the surface to around 4 at a depth of 3 m. The presence of a Hvorslev surface would limit the strength of the top of the clay foundation since it is likely to yield on the dry side of the critical state line. For the Schofield model, assuming that all other parameters are constant for a given soil, the s_u value depends only on the value of the maximum isotropic preconsolidation pressure p'_c. In order to specify the average s_u profile in a particular finite element analysis, the value of p'_c was adjusted based on the values of maximum preconsolidation pressures inferred from the vane shear strength profiles (Fig. 2(b)). Most of the critical state parameters for kaolin were taken from Al-Tabbaa (1987) and Stewart (1989). The value of coefficient of earth pressure at rest (K_0) at various depths for clay foundation was estimated based on the following equation proposed by Schmidt (1966):

$$K_0 = K_{onc}(OCR)^{1.2 \sin \phi'_{PS}}, \tag{4}$$

where K_{onc} is the coefficient of earth pressure at rest for normally consolidated clay and ϕ'_{PS} is the plane strain angle of internal friction for the clay foundation. Near the top of the clay foundation, the value of K_0 was limited to K_p (passive earth pressure coefficient).

For the analyses involving wick drains, the matching procedure suggested by Hird et al. (1992) was used to calculate equivalent plane strain horizontal permeability of the clay foundation. According to Hird et al. (1992), for the rate of consolidation in a plane strain and an axisymmetric case to be matched, it is necessary that the average degree of consolidation at every time and every level in the clay are equal. This condition can be expressed mathematically as

$$\frac{k_{PL}}{B^2 \mu_{PL}} = \frac{k_{AX}}{R^2 \mu_{AX}}, \tag{5}$$

where k is the permeability of the clay layer; subscripts PL and AX stand for plane strain and axisymmetric cases respectively; B is the half-width of the plane-strain unit cell; R is the radius of the axisymmetric unit cell and μ_{PL} and μ_{AX} are dimensionless factors. Based on Eq. (5), three different types of matching, i.e. geometric matching, permeability matching and combined matching can be achieved. For geometry matching, the values of permeability in plane strain and axisymmetric cases are kept the same. For permeability matching, B is taken equal to R. For combined matching, a value of B is pre-selected on the basis of required plane strain mesh refinement and then the value of k_{PL} is adjusted so that Eq. (5) can be satisfied. For the analyses presented here, in calculating the equivalent plane strain horizontal permeability of clay foundation, the combined matching procedure was adopted. B was taken equal to 2.25 m, R was taken equal to 0.65 m and k_{AX} was taken equal to

Table 2
Parameters specified for the finite element analyses[a]

			Soil–reinforcement interfaces	
Clay foundation	Sand embankment	Geotextile	Clay–geotextile	Sand–geotextile
$\kappa = 0.028$	$E = 4500$–$10\,000$	$E_r = 2.3\text{E} + 6$	$c = 10$	$c = 0.0$
$\lambda = 0.187$	$v = 0.3$	$v = 0.2$	$\phi = 0^\circ$	$\phi = 35^\circ$
$M = 0.755$	$\gamma = 16.0$	$A_r = 0.00212$	$K_n = 3500$	$K_n = 13\,000$
$\Gamma = 3.00$	$c = 0.1$		$K_s = 1000$	$K_s = 3800$
$v = 0.3$	$\phi = 35$ or 50°		$K_{sres} = 10$	$K_{sres} = 40$
$\gamma = 16.3$				
$k_x = 1.28\text{E} - 9$				
$k_y = 0.50\text{E} - 9$				
$H = 0.59$				
$S = 2.00$				
$k_{PL} = 6.55\text{E} - 9$				

[a] A_r — area of cross-section per meter width of the reinforcement (m^2/m); c — cohesion (kPa); E — Young's modulus of the sand embankment (kPa); E_r — Young's modulus of the reinforcement (kPa); H — slope of the Hvorslev surface in V–q–p' space; K_n — normal stiffness of the slip element (kPa); k_{PL} — equivalent plane strain horizontal permeability of clay (m/s); K_s — shear stiffness of the slip element (kPa); K_{sres} — residual stiffness of the slip element after slip (kPa); k_x — horizontal permeability of clay (m/s); k_y — vertical permeability of clay (m/s); S — slope of the tension cut-off surface in V–q–p' space; ϕ — angle of friction (degree); Γ — critical state specific volume at $p' = 1$ kPa; γ — bulk density (kN/m^3); η — stress ratio (q/p'); κ — slope of the swelling line in V–ln p' space; λ — slope of the compression line in V–ln p' space; M — slope of the critical state line in q–p' space; v — Poisson's ratio.

1.28×10^{-9} m/s (Al-Tabbaa, 1987). Table 2 lists the parameters specified for the clay foundation.

4.2. Modelling the sand embankment

The sand embankment was modelled as elastic-perfectly plastic material with a Mohr–Coulomb yield criterion and associated flow rule. Table 2 gives all the parameters specified for the sand embankment. The sand embankment was constructed in six layers. The elastic stiffness of each layer was specified in such a way that the lowermost layer had the highest elastic stiffness. However, no testing was done to obtain the elastic stiffness of each layer and the specified values are approximate. It has been pointed out by several researchers (e.g. Kwok, 1987; Rowe and Soderman, 1987) that the elastic stiffness of the embankment material has little influence on the overall behaviour of reinforced embankments as predicted by finite element analyses. This conclusion is based on the observation that the sand embankment modelled by an elastic-perfectly plastic model yields almost everywhere in each layer at the end of its construction which would indicate that the strength parameters have significantly greater influence on its behaviour than the elastic stiffness. A small value of cohesion $c = 0.1$ kPa was specified in order to avoid numerical instabilities at the toe of the

embankment. A critical state angle of internal friction (35° — derived from Sun, 1990) was used for the unreinforced embankment since large strains were expected at later stages of the analysis when the embankment construction is close to completion whereas a higher angle of internal friction (50° — derived from Mak, 1983) was used for the reinforced embankments to take into account the increase in strength due to dilation at small strains which were anticipated to be present throughout the analysis. A better option would have been to use an elastic-perfectly plastic model with a non-associated flow rule to represent the sand embankment. The average bulk unit weight of sand embankment achieved during centrifuge testing was 17.1 kN/m^3. However, the unit weight was reduced to 16 kN/m^3 to compensate for the calculated friction between the sand and the inner sides of the strongbox (Sharma, 1994). The friction between the sand and the inner sides of the strongbox was estimated using the coefficients of friction obtained using shear box tests (Balachandran, 1996) and an active condition was assumed in the embankment for the estimation of normal forces on the inner sides of the strongbox.

4.3. Modelling the reinforcement and its interfaces with soil

As mentioned above, the geotextile reinforcement was modelled using linear elastic bar elements. The stiffness of the reinforcement was derived from the load-elongation curve obtained by carrying out 1%/min tensile tests on 200 mm wide specimens with 200 mm gauge length. Table 2 gives the parameters specified for the reinforcement. It should be noted that the stiffness of the reinforcement (usually denoted by J and having unit of kN/m) is equal to its Young's modulus E_r multiplied by the area of cross-section A_r.

The soil–reinforcement interfaces were modelled using the six-noded quadrilateral interface elements. The parameters specified for the interfaces are tabulated in Table 2. The sand–reinforcement interface was considered purely frictional whereas the clay-reinforcement interface was considered purely cohesive. The parameters for the sand–reinforcement interface were derived from a series of direct shear tests done by Balachandran (1996). A value of cohesion equal to the undrained shear strength of the clay foundation near its surface was specified for the clay–reinforcement interface. For both these interfaces, the elastic normal and shear stiffness were taken equal to those of the adjacent soil layers.

4.4. Outline of the analyses

Three analyses were carried out in the present study. Table 3 gives the details of these analyses. For all the analyses, the embankment construction was carried out in six stages (one layer per stage). The total time allowed for embankment construction was 6 days and 3 h. The reader should note that the comparisons between experimental and numerical results are presented at prototype scale. The scaling laws that relate the behaviour of a centrifuge model to the behaviour of its prototype can be found in Schofield (1980).

Table 3
Details of the finite element analyses

Analysis identifier	Reinforcement	Wick drain
REWD1	Geotextile	Not present
REWD3	None	Not present
REWD5	Geotextile	Present

5. Results and comparisons

5.1. Collapse height of unreinforced embankment

Fig. 8(a) shows the horizontal displacement of node 158 (located in the clay layer close to the toe of the embankment) as computed by analysis REWD3. As mentioned previously, in the centrifuge test JSS8, the clay foundation failed when 85% of the total weight of sand contained in the hopper was placed on its surface. Analysis REWD3 computes this figure as 86% as seen from Fig. 8(a). It is evident from such a close comparison between the measured and computed failure height of the embankment that the specification of an average s_u profile as described above has modelled the behaviour of one-dimensionally consolidated anisotropic clay foundation fairly accurately. Further evidence of the success of this procedure can be seen from Fig. 8(b) showing the contours of stress ratio $\eta(q/p')$ and Fig. 8(c) showing contours of mobilised shear stress at the onset of failure (increment 465). In the shaded region of Fig. 8(b), the value of η is equal to M which indicates that almost the entire clay foundation is at critical state. When this shaded region is superimposed on the contours of mobilised shear stress in Fig. 8(c), it can be seen that up to 16 kPa of shear stress was mobilised at failure which is slightly higher than the specified undrained shear strength of the clay foundation. This is due to the fact that the clay foundation, which is modelled using coupled-consolidation elements, gained strength due to consolidation during the embankment construction.

5.2. Displacement of clay foundation

In this section, the results obtained from analyses REWD1 and REWD5 are compared with the results obtained from the centrifuge tests JSS7 and JSS14, respectively. Fig. 9(a) shows the comparison between the horizontal displacement of the clay foundation immediately after the end of embankment construction at two "inclinometer" locations, each consisting of a column of black plastic markers in the case of centrifuge tests and a column of nodes for the finite element analyses. It can be seen from Fig. 9(a) that there is a close agreement between the observed and the computed horizontal displacements for both tests JSS7 and JSS14. However, the computed horizontal displacements near the surface of the clay foundation were marginally less than the observed horizontal displacement whereas those computed

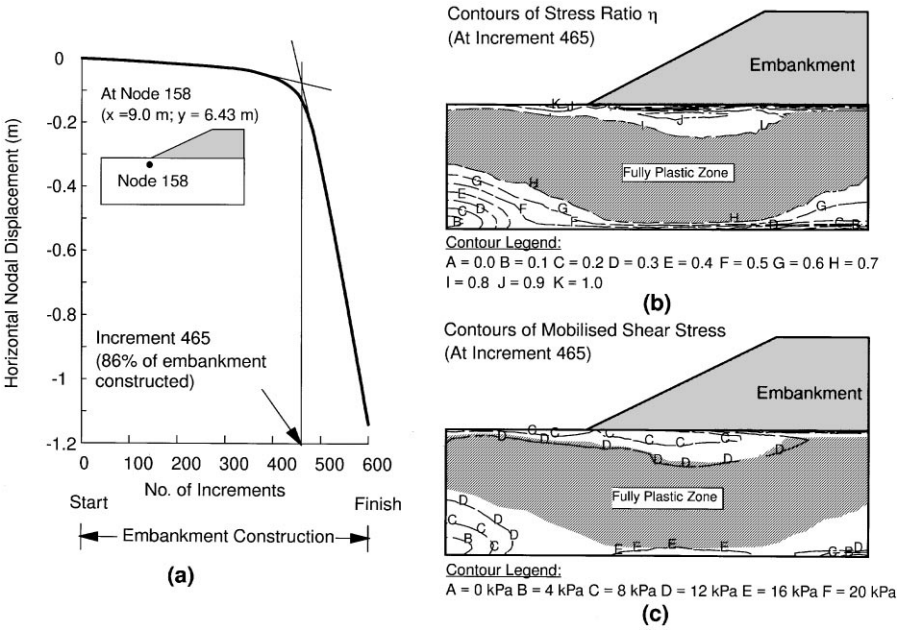

Fig. 8. (a) Computed horizontal displacement near the toe of the embankment (Analysis REWD3). (b) Distribution of stress ratio η at failure (analysis REWD3). (c) Contours of mobilized shear stress at failure (analysis REWD3).

near the bottom of the clay foundation were slightly larger than the observed horizontal displacements.

The comparison between the computed and observed vertical displacement of the clay foundation close to its top surface immediately after the end of embankment construction are shown in Fig. 9(b). The computed settlements under the shoulder of the embankment and the computed heave beyond the toe of the embankment are quite close to the observed values for both tests JSS7 and JSS14. However, the computed settlements under the slope of the embankment are less than the observed settlements and those computed under the centreline of the embankment are considerably greater than the observed values. The observed settlements near the centreline of the embankment may have been influenced by the presence of the geotextile clamp (see Fig. 1) shielding the clay from the sand above.

5.3. *Excess pore pressures in the clay foundation*

Fig. 10 shows the variation of excess pore pressure during embankment construction measured during tests JSS7 and JSS14. Superimposed on the measured variation are the variations computed by analyses REWD1 and REWD5. For the case of no wick drain, there was a good agreement between the measured and computed variation towards the end of embankment construction. However, the measured and

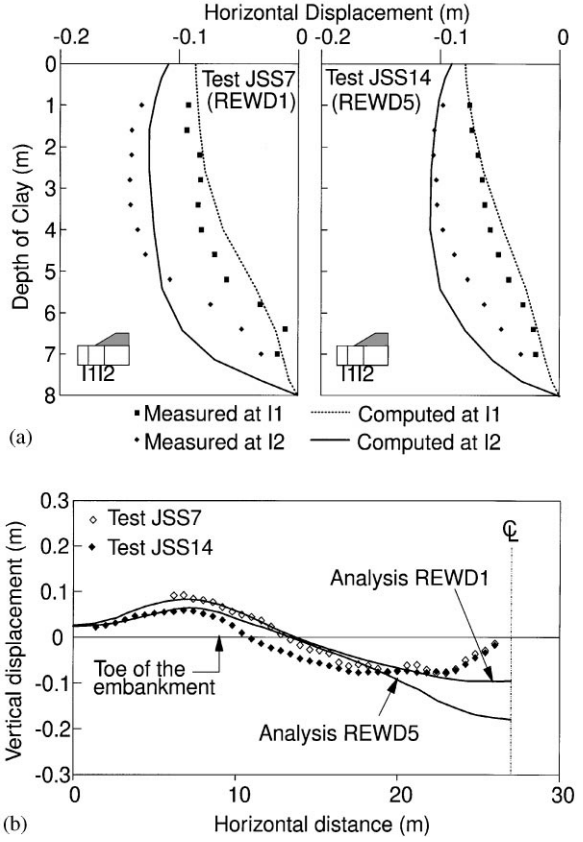

Fig. 9. (a) Measured and computed horizontal displacements of the clay foundation at the end of embankment construction. (b) Measured and computed vertical displacements of the clay foundation at the end of embankment construction.

computed values of excess pore pressure showed some difference during the middle of the embankment construction. This may be attributed to the fact that in the finite element analyses, the embankment was constructed in six layers but in the centrifuge test, it was constructed in 20 layers. It should be pointed out that in the centrifuge test, some of the embankment layers were quite thin and therefore, an exact simulation of the construction process would have rendered some elements with extreme length to width ratios and would have introduced numerical ill-conditioning into the analyses.

For the case of wick drains, the measured and computed values of excess pore pressure appear to be in good agreement towards the end of embankment construction. It is important to realise that the matching procedure proposed by Hird et al. (1992) does not result in the excess pore pressures at corresponding points in axisymmetric and plane strain unit cells to be the same. However, the discrepancy between the two is negligible in the middle one-third portion of the unit cell (from $0.3R$ to $0.6R$

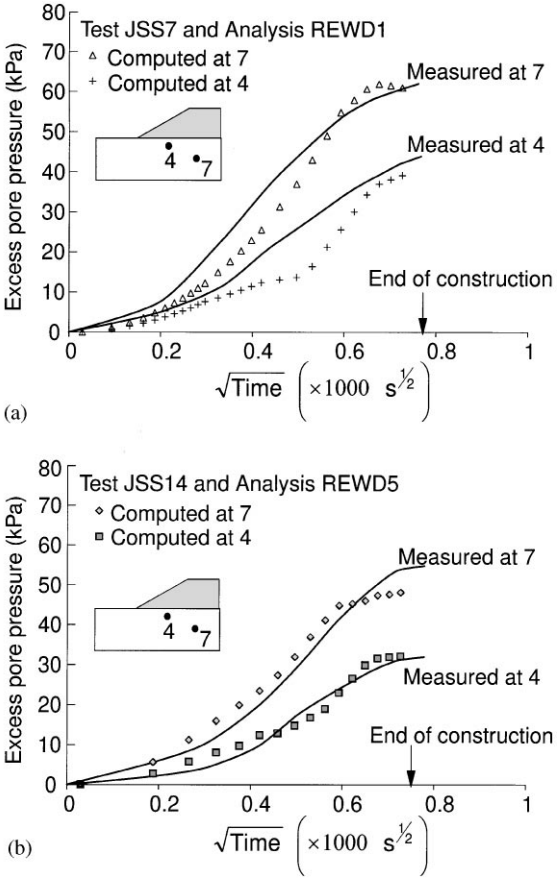

Fig. 10. Measured and computed excess pore pressures in the clay foundation during embankment construction.

for axisymmetry or from $0.3B$ to $0.6B$ for plane strain). The two pore pressure measurement points (4 and 7) shown in Fig. 10 are located in this range. If the unavoidable discrepancy between the measured and computed excess pore pressure values close to wick drains is ignored, the overall distribution of excess pore pressure was very similar for the centrifuge test and the finite element back-analysis. This confirms the applicability of the equivalent permeability calculated by the combined matching procedure suggested by Hird et al. (1992).

5.4. Tension in the reinforcement

Fig. 11(a) shows the measured tension profiles in the reinforcement along the width of the embankment for tests JSS7 and JSS14. Also depicted in Fig. 11(a) are the tension profiles in the reinforcement computed by analyses REWD1 and REWD5.

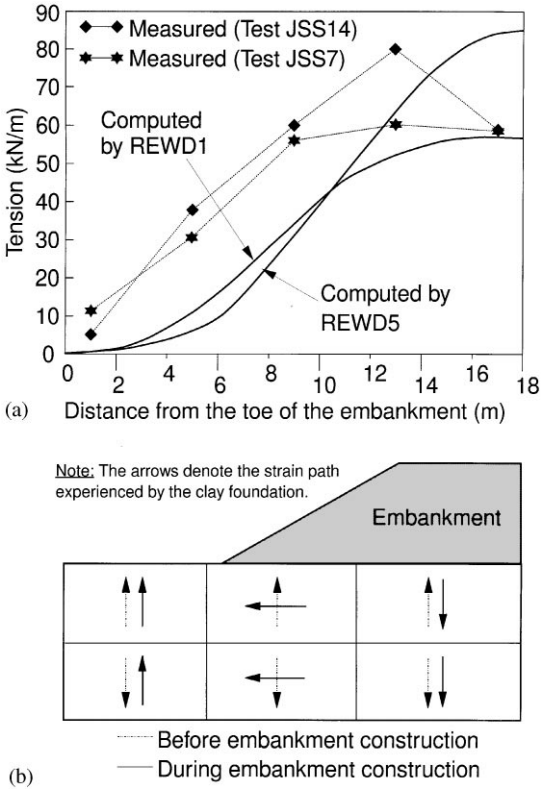

Fig. 11. (a) Measured and computed tension in the reinforcement. (b) Strain paths in the clay foundation before and during embankment construction.

There is close agreement between the computed and measured value of maximum tension in the reinforcement. Also, the computed distribution of tension in the reinforcement along the width of the embankment shows trends that are similar to those observed in the centrifuge models. However, the computed tensions show localisation under the shoulder of the embankment. Their values are less than the observed tension values underneath the slope of the embankment. The localisation of computed tensions is much more pronounced for analysis REWD5 (with wick drains). It is worth noting that for test JSS14 (with wick drains), the tensions in the reinforcement were also observed to be more localised under the shoulder of the embankment as compared with the tensions observed in test JSS7 (without wick drains).

The discrepancy between the computed and measured values of tension in the reinforcement underneath the slope of the embankment can be explained with the help of Fig. 11(b) showing the strain paths experienced by the clay foundation before and after the construction of the embankment. For a typical centrifuge test in the present study, the top half of the clay foundation reached a state of equilibrium by continuous swelling. Therefore, when the embankment was constructed, the clay in

the passive zone (away from the embankment) continued to swell, the clay in the shear zone (underneath the slope of the embankment) experienced approximately 90° rotation of the strain path and the clay in the active zone (underneath the shoulder of the embankment) experienced a complete reversal of the strain path. Therefore, the stiffness of the clay deteriorated significantly in the passive and shear zones thus inducing greater strains in the portion of reinforcement lying underneath the slope of the embankment.

6. Discussion

As mentioned previously, analysis REWD3 (unreinforced) predicted the failure of the embankment at the completion of 86% of the embankment whereas analysis REWD1 (reinforced) predicted only 0.12–0.13 m of lateral movement at the end of embankment construction. An examination of the distribution of stress ratio η in the clay foundation immediately after the end of embankment construction for analysis REWD1 (Fig. 12) reveals that almost the entire clay foundation is at a critical state ($\eta = M$ in the shaded "fully plastic zone"). This indicates that the mobilized shear stress is equal to available shear strength almost everywhere in the clay foundation and yet the embankment remains serviceable. The only component preventing the embankment from failing is the reinforcement. However, the contribution of the mobilized shear stress of the clay foundation towards the stability of the embankment far outweighs the contribution of the mobilized tension in the reinforcement. For most practical cases, it can be easily demonstrated using a simple limit equilibrium slip circle analysis (e.g. Low et al., 1990) that the proportion of restoring moment provided

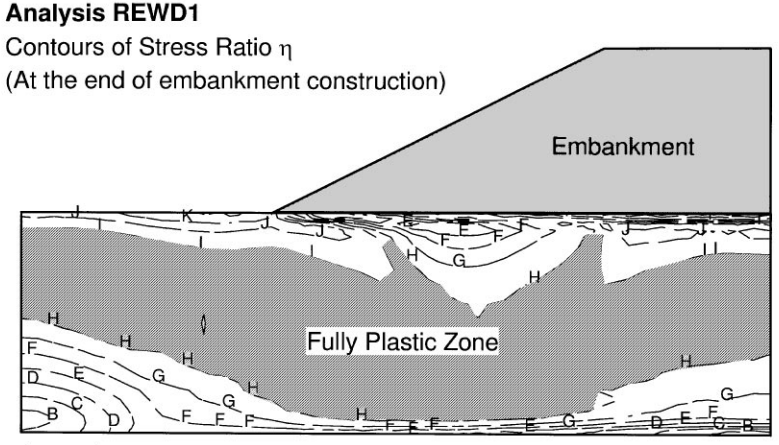

Fig. 12. Distribution of stress ratio η at the end of embankment construction (analysis REWD1).

by the mobilised shear stress (s_{mob})in the clay is much more than that provided by the mobilised tension in the reinforcement (T_{mob}). This is because of the fact that s_{mob} when integrated over the entire length of the slip circle is much larger in magnitude than T_{mob} and it also has a longer lever arm as compared to that for T_{mob}. Therefore, if the available shear strength of the clay foundation is significantly less than the required shear strength, the reinforcement has to mobilize a tensile force of rather large magnitude in order to make the restoring moment equal to the disturbing moment. In most situations, this may not be possible because of unavoidable shear failure at the clay-reinforcement interface and the accompanying large deformations. In these situations, increasing the available shear strength of the clay foundation by installation of wick drains appears to be a viable option. When wick drains are used in combination with a geosynthetic base reinforcement, the advantages are two-fold. A higher degree of consolidation of the clay foundation achieved during the embankment construction would ensure higher available shear strength of clay foundation. This in turn would favour better mobilization of tension in the reinforcement due to a stronger clay–reinforcement interface.

7. Conclusions

The behaviour of a reinforced embankment on soft clay installed with wick drains has been successfully investigated using centrifuge modelling and finite element analyses. Reasonably good comparisons between the measured and the computed results have emphasised the importance of taking into account the stress-induced anisotropy of the clay foundation. The concept of using an equivalent value of horizontal permeability based on the matching procedure suggested by Hird et al. (1992) was successful in the modelling of the clay foundation installed with wick drains.

For the case of reinforced embankments on soft clay installed with wick drains, it was found that the magnitude of maximum tension in the reinforcement was slightly higher than that for the case of no wick drains. Also, the distribution of tension in the reinforcement was much more localised under the shoulder of the embankment for the wick drain case as compared to the case of no wick drains. This is consistent with the observation that the displacement of clay foundation installed with wick drains is also concentrated under the shoulder of the embankment. Lateral spreading is one of the main cause of concern for embankments founded on soft clays. The results of the centrifuge tests and finite element back-analyses have indicated that the installation of wick drains limits the extent of lateral spreading of the clay foundation at the expense of slightly higher tension in the reinforcement and slightly greater settlement underneath the shoulder of the embankment.

When wick drains are used in combination with a geosynthetic base reinforcement, the advantages are two-fold. A higher degree of consolidation of the clay foundation achieved during the embankment construction would ensure higher available shear strength of clay foundation. This in turn would favour better mobilization of tension in the reinforcement due to a stronger clay–reinforcement interface.

Acknowledgements

The experimental part of the work described in this paper was funded by the Transport Research Laboratory, UK. The help and technical support of the staff of the Schofield Centrifuge Centre and the Soil Mechanics Laboratory of Cambridge University is gratefully acknowledged. The authors wish to thank Dr. Arul Britto for his useful suggestions on the finite element modelling. The first author is grateful for the financial support provided by the Nehru Trust for Cambridge University and the ORS award given by the CVCP of British Universities for his doctoral studies.

References

Almeida, M.S.S., Parry, R.H.G., 1983. Studies of vane and penetrometer tests during centrifuge flight. Technical Report No. TR142, Cambridge University Engineering Department, UK.

Al-Tabbaa, A., 1987. Permeability and stress–strain response of speswhite kaolin. Ph.D. Thesis, Cambridge University Engineering Department, UK.

Balachandran, S., 1996. Modelling of geosynthetic reinforced soil walls. Ph.D. Thesis, Cambridge University Engineering Department, UK.

Bassett, R.H., Yeo, K.C., 1988. The behaviour of a reinforced trial embankment on soft shallow foundation. Proceedings of the International Geotechnical Symposium on Theory and Practice of Earth Reinforcement, Fukuoka, Japan, pp. 371–376.

Blight, G.E., 1968. A note on field vane testing of silty soils. Can. Geotech. J. 5, 142–149.

Bolton, M.D., Sharma, J.S., 1994. Embankments with base reinforcement on soft clays. Proceedings of the Centrifuge'94 conference, Singapore, pp. 587–592.

Britto, A.M., Gunn, M.J., 1990. CRISP90 — User's and Programmer's Guide, Vols. 1 & 3. Cambridge University Engineering Department, UK.

Broms, B.B., Chu, J., Choa, V., 1994. Measuring the discharge capacity of band drains by a new drain tester. Proceedings of Fifth International Conference on Geotextiles, Geomebranes and Related Products, Singapore, Vol. 2. pp. 803–806.

Goodman, G.E., Taylor, R.L., Brekke, T.L., 1968. A model for the mechanics of jointed rock. J. Soil Mech. Found. Engng. Div. ASCE 94, 637–659.

Hird, C.C., Pyrah, I.C., 1991. Predictions of the behaviour of a reinforced embankment on soft ground. Proceedings of the International Conference on the Performance of Reinforced Soil Structures, Glasgow, UK, pp. 409–414.

Hird, C.C., Pyrah, I.C., Russell, D., 1992. Finite element modelling of wick drains beneath the embankments on soft ground. Géotechnique 42 (3), 499–511.

Hird, C.C., Pyrah, I.C., Russell, D., Cinicioglu, F., 1995. Modelling the effect of vertical drains in two-dimensional finite element analyses of embankments on soft ground. Can. Geotech. J. 32, 795–807.

Kwok, C.M., 1987. Reinforced embankments on soft ground. Ph.D. Thesis. University of Sheffield, UK.

Ladd, C.C., Foott, R., 1974. New design procedure for stability of soft clays. J. Geotech. Engng. Div. ASCE 100, 763–786.

Low, B.K., Wong, K.S., Lim, C., Broms, B.B., 1990. Slip circle analysis of reinforced embankments on soft ground. Geotex Geomem. 9 (2), 165–181.

Mak, K.W., 1983. Modelling the effects of a strip load behind rigid retaining walls. Ph.D. Thesis. Cambridge University Engineering Department, UK.

Ohta, H., Nishihara, A., Morita, Y., 1985. Undrained stability of K_0-consolidated clays. Proceedings of Eleventh International Conference on Soil Mechanics and Foundation Engineering, San Francisco, Vol. 2. pp. 613–617.

Ohta, H., Nishihara, A., Iizuka, A., Morita, Y., 1992. Use of field vane data in the analysis of soft clay foundations. Proceedings of the Wroth Memorial Symposium on Predictive Soil Mechanics, Thomas Telford, London, pp. 387–405.

Phillips, R., 1988. Centrifugal lateral pile tests in clay: Tasks 2 & 3. A report to Exxon Product Research Corporation by Lynxvale Ltd., Cambridge, UK.

Prevost, J.H., 1979. Undrained shear tests on clays. J. Geotech. Engng. Div. ASCE 105, 49–64.

Rowe, R.K., Gnanendran, C.T., Landva, A.O., Valsangkar, A.J., 1995. Construction and performance of a full-scale geotextile reinforced test embankment, Sackville, New Brunswick. Can. Geotech. J. 32, 512–534.

Rowe, R.K., Mylleville, B.L.J., 1989. Consideration of strains in the design of reinforced embankments. Proceedings of Geosynthetics'89 Conference, San Diego, pp. 124–135.

Rowe, R.K., Soderman, K.L., 1987. Stabilization of very soft soils using high strength geosynthetics: the role of finite element analyses. Geotex. Geomem. 6, 53–80.

Schmidt, B., 1966. Discussion of Earth pressure at rest related to stress history by Booker and Ireland (1965). Can. Geotech. J. 3 (4), 239–242.

Schofield, A.N., 1980. Cambridge University geotechnical centrifuge operations. Géotechnique 30 (3), 227–268.

Sharma, J.S., 1994. Behaviour of reinforced embankments on soft clay. Ph.D. Thesis, Cambridge University Engineering Department, UK.

Sharma, J.S., Bolton, M.D., 1996. Finite element analysis of centrifuge tests on reinforced embankments on soft clay. Comput. Geotech. 19 (1), 1–22.

Springman, S.M., 1989. Lateral loading in piles due to simulated embankment construction. Ph.D. Thesis, Cambridge University Engineering Department, UK.

Springman, S.M., Bolton, M.D., Sharma, J., Balachandran, S., 1992. Modelling and instrumentation of a geotextile in the geotechnical centrifuge. Proceedings of the International Symposium on Earth Reinforcement Practice, Fukuoka, Japan, pp. 167–172.

Stewart, D.I., 1989. Groundwater effects on in-situ walls in stiff clays. Ph.D. Thesis, Cambridge University Engineering Department, UK.

Sun, H.W., 1990. Ground deformation mechanisms for soil structure interaction. Ph.D. Thesis. Cambridge University Engineering Department, UK.